THE ASTROPHYSICAL JOURNAL, 431:402–415, 1994 August 10

X-RAY EMISSION ON HYBRID STARS: *ROSAT* OBSERVATIONS OF α TRIANGULI AUSTRALIS AND ι AURIGAE

V. KASHYAP
Department of Astronomy and Astrophysics, University of Chicago, 5640 South Ellis Avenue, Chicago, IL 60637
R. ROSNER
Department of Astronomy and Astrophysics and Enrico Fermi Institute, University of Chicago, 5640 South Ellis Avenue, Chicago, IL 60637
F. R. HARNDEN, JR.
Harvard-Smithsonian Center for Astrophysics, 60 Garden Street, Cambridge, MA 02138
AND
A. MAGGIO, G. MICELA, AND S. SCIORTINO
Osservatorio Astronomico di Palermo, Palazzo dei Normanni, 90134 Palermo, Italy
Received 1993 September 13; accepted 1994 February 9

ABSTRACT

We report on deep *ROSAT* observations of two Hybrid atmosphere stars, α TrA and ι Aur, and our analysis of these observations. We detect high-energy transient phenomena on α TrA and consider the implications of this discovery to the atmospheres of Hybrid stars. We detect ι Aur in the high-energy passband of *ROSAT*, implying the existence of multimillion degree plasma on the star. Our major results include the following: discovery of two large flare events, detected during pointed observations of α TrA; the demonstration that the flare emission most likely comes from the giant itself, rather than from a previously unseen low-mass companion star; the demonstration that the plasma characteristics associated with the flares and with the "quiescent" component are essentially indistinguishable; and that the geometric dimensions of the emitting plasma are considerably smaller than the critical dimension characterizing stable "hot" coronal loop structures. Our results suggest that α TrA does not have any steady X-ray emission, consistent with theoretical expectations, and support the argument that Hybrid stars constitute a transitional type of object in which large-scale magnetic dynamo activity ceases, and the dominant spatial scales characterizing coronal structure rapidly decline as such stars evolve across the X-ray "Dividing Line" in the H-R diagram.

Subject headings: stars: coronae — stars: flare — stars: individual (α Trianguli Australis, ι Aurigae)

1. INTRODUCTION

It was first recognized by Linsky & Haisch (1979) that stars on the giant branches of the H-R diagram undergo a transition in the characteristics of their atmospheres. They identified a "Dividing Line" in the H-R diagram wherein stars to the left of the line exhibited spectral lines formed at temperatures of $\sim 2 \times 10^5$ K (indicating the existence of chromospheres, transition regions, and hence coronae) in their *IUE* spectra, while stars to the right showed no lines that formed at temperatures hotter than ~20,000 K. They speculated that this transition was a manifestation of changing magnetic field topology: a star with "closed" field lines would be brighter in X-rays than a star with "open" field lines and large winds, in analogy with the solar active region/coronal hole dichotomy. Later, using data from the *Einstein Observatory*, Ayres et al. (1981) extended this "Chromospheric Dividing Line" to a "Coronal Dividing Line" where some stars to the left of the line exhibited X-ray emission, while stars to the right did not. They also found that the Coronal Dividing Line coincided with a "Wind Dividing Line" (cf. Stencel et al. 1980) defined by a change in the asymmetry of Mg II h and k lines indicating the existence of mass loss via cool winds. The existence of the Coronal Dividing Line was subsequently verified in an extensive *Einstein* survey by Maggio et al. (1990). It has also been recently confirmed at higher sensitivities by Haisch, Schmitt, & Rosso (1991; see also Haisch, Schmitt, & Fabian 1992) using data from the all-sky survey conducted with the *ROSAT Observatory*. We will henceforth use the term "Dividing Line" to represent that region of the H-R diagram where all of the above-mentioned transitions—chromospheric, coronal and wind—occur.

In addition to the two types of giant stars on either side of the Dividing Line identified above ("solar-like" on the left and "non-solar-like" on the right), a third class of stars related to the Dividing Line was discovered by Hartmann, Dupree, & Raymond (1980): Hybrid-chromosphere stars (or more simply, Hybrid stars), which exhibited both evidence for a transition region (hence "solar-like") as well as signature of mass loss via a cool wind (hence "non-solar-like"). These stars[1] straddle the Dividing Line, and are possibly an intermediate evolutionary stage between the two extremes. Hybrid stars were not known to be X-ray emitters in general until the advent of *ROSAT*. With the exception of α TrA, which was detected with *EXOSAT* (Brown et al. 1991), no other Hybrid star had been observed in the X-ray regime. During the *ROSAT* All-Sky Survey, δ And was detected, in addition to α TrA, by Haisch, Schmitt, & Rosso (1992). Later, independent pointed *ROSAT* observations by Reimers & Schmitt (1992) lasting from ~5 to ~11 ks (~1.4–3 hr) succeeded in detecting three other Hybrid stars—β Ind, μ UMa, and γ Aql. With the detection of ι Aur (Kashyap et al. 1992a; this paper), every Hybrid star that

[1] Note that Hybrid stars are defined entirely in terms of *IUE* observations, as stars with detectable fluxes in C IV and other transition region lines, and exhibiting a high speed absorption component in Mg II emission-line profiles indicative of a stellar wind (Hartmann et al. 1980; Haisch 1987).

was observed during the pointed phase of the *ROSAT* program has been detected.[2]

Here we report on pointed *ROSAT* X-ray observations of two Hybrid stars, α TrA (cf. Hartmann et al. 1981) and ι Aur (cf. Reimers 1982), and consider the ramifications of our observations on theories proposed to explain the origin of the Dividing Line. We analyze our observations of the program stars in § 2. In § 2.1 we present our *ROSAT* observations, and in § 2.2 we analyze these observations. In § 3 we summarize previous X-ray and UV observations of these stars and discuss the stellar parameters we adopt. In § 4 we discuss our results and compare them with previous observations and models of X-ray emission in giant stars. In § 4.1 we consider the possibility that α TrA has an unseen dwarf companion; in § 4.2 we discuss the results of our observations of α TrA; and in § 4.3 we discuss our observation of ι Aur. We summarize our conclusions in § 5.

2. X-RAY DATA AND ANALYSIS

In this section we present the X-ray data obtained for our program stars using the *ROSAT Observatory*, and a description of our analysis of these data. For a summary of previous X-ray and UV observations of these stars, see § 3.

2.1. *ROSAT Observations*

In order to help constrain models for the change in X-ray emission across the Coronal Dividing Line, long duration X-ray observations of two similar, nearby Hybrid stars, α TrA and ι Aur, were carried out. The observations were purposely long in order to obtain good count statistics for spectral analysis. The data from these observations, obtained with the Position Sensitive Proportional Counter (PSPC-B) on the *ROSAT Observatory* (see Trümper et al. 1991), are analyzed below. Both observations were performed in 1991 September (after the conclusion of the All-Sky Survey) and spanned a time interval of about a day, roughly one-third of which contained usable data (i.e., data obtained outside the South Atlantic Anomaly and other high background intervals). In the case of ι Aur, the time intervals were further pruned to eliminate intervals of high background due to O V fluorescence. The parameters of the observations are listed in Table 1. Telescope wobble at an amplitude of ~3′ was on, and was stable throughout the observations.

2.2. *Analysis*

The data were first processed by the *ROSAT* Science Data Center with the Standard Analysis and Software System (SASS). The reduced data were subjected to further analysis by us as outlined below using the Post Reduction Offline System (PROS) in the IRAF environment and the Extended Scientific Analysis System (EXSAS) in the MIDAS environment. Detailed spectral analysis was performed using XSPEC. A summary of the results of the spatial and spectral analyses of the data for both α TrA and ι Aur for the entire observation is presented in Table 2. We will consider each star separately in further detail below.

[2] Arcturus, α Boo, was also observed during the pointed phase of *ROSAT* observations, but was not detected (Ayres, Fleming, & Schmitt 1991). It is now suspected that α Boo is also a Hybrid star (T. R. Ayres 1993, private communication), with very weak C IV emission, and X-ray fluxes below *ROSAT* sensitivity.

TABLE 1

ROSAT OBSERVATIONS OF α TrA (=HD 150798 = HR 6217) AND ι AUR (=HD 31398 = HR 1577)

Parameter	α TrA	ι Aur
Observation code	RP 200 548	RP 200 547
Detector	PSPC 2 (B)	PSPC 2 (B)
Filters	None	None
Start of observation	1991 Sep 21 $14^h59^m10^s$ UT	1991 Sep 04 $23^h22^m5^s$ UT
End of observation	1991 Sep 22 $18^h23^m11^s$ UT	1991 Sep 05 $23^h15^m57^s$ UT
Number of OBIs	2	2
ON time	31.577 ks	28.734 ks
Total accepted time	31.577 ks	26.400 ks
Field center, $(R.A., Decl.)_{2000}$	(252°.17, −69°.03)	(74°.25, 33°.17)
Field center, (l, b)	(321°.53, −15°.26)	(170°.59, −6°.16)

2.2.1. α *TrA*

Our *ROSAT* data span approximately a day, in segments called Good Time Intervals (GTIs) of varying size with a total of $\approx 8\frac{3}{4}$ hr. We have confined our analysis to the energy range 0.17–2.02 keV. Applying the LDETECT task of PROS to these data leads to an unambiguous detection of an X-ray source at the position ($16^h48^m40^s.3$, −69°1′46″), at a signal-to-noise ratio of ~52. This source is ≈10″ away from the optical position, ($16^h48^m39^s.8$, −69°1′39″) of α TrA, consistent with the magnitude of position errors for the PSPC (cf. Micela et al. 1994).[3] We thus detect α TrA as a strong X-ray source. For all further spectral and temporal analyses, we extract the photons from within a circle of radius 50″ centered at this position. At photon energies of 0.17 keV, 94% of the source counts lie within this circle, and at higher energies, essentially all the source counts lie within it. The background is evaluated in an annulus outside this circle, extending to 3′. Other X-ray sources that overlap this annulus are excised from it. With this method, we obtain 3730 ± 62 counts from α TrA (the background is 130.4 ± 3.7), for an average count rate of 0.12 counts s^{-1}. There is some uncertainty as to whether the detected star is α TrA or a dwarf companion, and this question is addressed in § 4.1. We find it more likely that we have indeed detected the Hybrid star and will analyze our results based on that assumption.

The large number of counts obtained allows us to analyze the temporal variation of the X-ray emission from this star. In Figure 1 we plot the count rate in each GTI as a function of the midsegment time value as measured from the beginning of the observations.[4] The X-ray light curve exhibits two distinct types

[3] Unfortunately, there is no way to estimate the positioning errors independently within the observation, as there is no other X-ray source in the field of view that can be unambiguously identified with an optical source.

[4] We obtain the count rate by dividing the counts (obtained as described above) in the given GTI by the exposure time from an exposure map generated using EXSAS, averaged over ~5 pixels of the map in the neighborhood of the source. The exposure times thus calculated differ from the actual ON time by ≲3% over the entire observation, with deviations of as much as 6%. This is within the expected range of variations in the exposure times calculated for *ROSAT* (cf. Micela et al. 1994). Note that the "wobbling" of the spacecraft (designed to achieve a uniform exposure of the sky in the neighborhood of the spacecraft pointing) introduces a modulation of the source counts due to repetitive occultation of sources in the field of view by the wire mesh that is part of the window support structure. This modulation is on timescales ~10^2 s, and can lead to spurious detections of variability in a source if not properly accounted for. We therefore emphasize that our further analysis (see below) is confined to timescales ≫10^2 s, over which the exposure of a given piece of sky is uniform. Hence, the modulation introduced by the wobbling is *not* relevant here.

TABLE 2

SUMMARY OF INITIAL X-RAY ANALYSIS

Parameter	α TrA	ι Aur
PI bins used	17:202	28:202
Net counts	3730 ± 62	20.7 ± 5.6
Background counts	130.4 ± 3.7	8.3 ± 1.7
Spectral fit parameters:[a]		
Column density ($\times 10^{19}$ cm^{-2})	$4.6^{+2.15}_{-1.6}$ [b]	...
	$3.2^{+2.36}_{-1.83}$ [c]	...
	$6.3^{+4.4}_{-2.8}$ [d]	...
High temperature, T_H (keV)	$1.21^{+0.22}_{-0.19}$ [b]	...
	$1.21^{+0.41}_{-0.18}$ [c]	...
	$1.16^{+0.24}_{-0.13}$ [d]	...
Low temperature, T_L (keV)	$0.29^{+0.05}_{-0.06}$ [b]	...
	$0.33^{+0.09}_{-0.08}$ [c]	...
	$0.25^{+0.08}_{-0.05}$ [d]	...
Flux (0.1–2.4 keV) (ergs s^{-1} cm^{-2})	1.1×10^{-12} [b]	6.1×10^{-15} [e]
	8.7×10^{-13} [c]	...
	1.5×10^{-12} [d]	...

[a] The limits quoted are 90% confidence intervals on the fit parameters, and are derived in XSPEC(v8) with the PSPC response matrix of 1992 March 11.

[b] For entire data set.

[c] For the duration of the observation *excluding* the two identified flares.

[d] For the duration of the two identified flares.

[e] Obtained using a conversion factor determined from spectral analysis of α TrA.

of behavior: a large-amplitude transient event dominating the first half of the light curve, and smaller-amplitude fluctuations evident in the remaining time.

We first focus on the large transient "events" seen in the early part of the light curve (i.e., during the interval $> +4$ hr and $< +12$ hr; cf. Fig. 1). Here the departure from source constancy is extremely large, with a reduced $\chi^2 \approx 27$ for a constant source model. An attempt to fit the transient "event" with a *single* exponentially decaying component results in a poor fit (goodness of fit, $q \ll 0.001$). Fitting the same data with *two* exponentially decaying components does improve the fit significantly: the *e*-folding decay timescales of what appear to be two successive flares are 3.2 ± 0.3 hr ($q = 0.96$) and 4.7 ± 0.9 hr ($q = 0.84$). These fits were carried out using the routines given in Press et al. (1986). Note that these decay timescales are consistent (for a plasma at $\gtrsim 10^7$ K; see below) with electron number densities $\approx 10^{10}$ cm^{-3}.

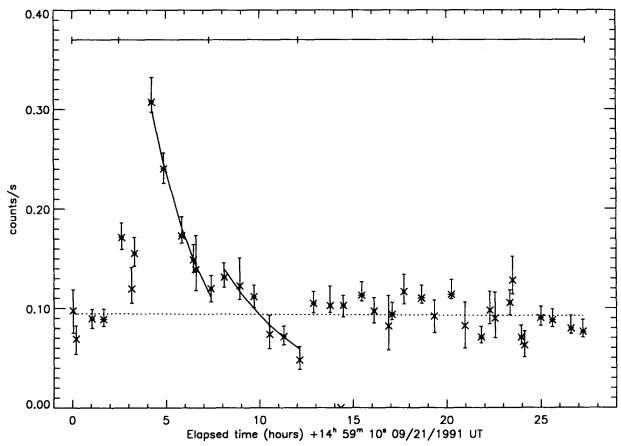

FIG. 1.—Background-subtracted light curve of α TrA. We plot the count rate in each GTI as a function of the elapsed time from the beginning of the observations (*crosses*). Also plotted (*vertical bars*) are 2 σ errors on the count rates, the mean "quiescent" flux (*dotted line*), and the best-fit decay curves for the two flares (*solid curves*). The thin solid horizontal line at the top of the graph shows the duration of the five subintervals used in the spectral analysis (cf. Fig. 4). The horizontal solid line segments bisecting the crosses indicate the duration of each GTI.

Next, we focus on the time interval characterized by the smaller-amplitude fluctuations. If we restrict our attention only to these fluctuations (i.e., to times $< +4$ hr and $> +12$ hr; cf. Fig. 1), then the count rates calculated for each GTI reveal a mean "quiescent" emission rate of 0.093 ± 0.008 counts s^{-1}. The large reduced χ^2 obtained for a straight-line fit to these count rates (~ 2 for 26 degrees of freedom) reinforces the impression of considerable short-term, low-intensity variability. This is verified when a more powerful technique to determine source variability is applied to the data, such as the method of phase-averaged reduced χ^2 (Collura et al. 1987). This technique is well suited for the analysis of low count rate sources with significant gaps in the data stream. (For a short description of the technique see Appendix A). The photon arrival time data are used to compare the observed data to expected "constant" source count rate models.[5] Computing the phase-averaged reduced χ^2 at various bin sizes (Collura et al. 1987; cf. Appendix A) for the data acquired during the "quiescent" phase of the emission, we find a fractional effective variability at a level of ~ 0.1 at bin sizes exceeding 7 ks (~ 2 hr) at confidence levels $\gtrsim 95\%$ (Fig. 2). (A similar calculation performed for the time interval with the two identified flares yields a fractional effective variability ~ 0.5 at high confidence levels $\sim 99\%$.)

[5] At this point, the repetitive occultations of the source due to spacecraft wobbling (alluded to above) might be thought to influence the data and result in spurious detections of variability. However, this is not the case, since this method allows us to obtain an estimate of the timescale of the variability, and we show below that this timescale is much greater than $\sim 10^2$ s.

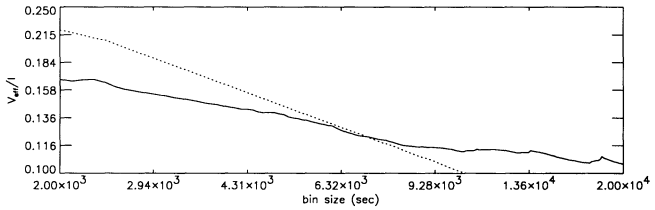

FIG. 2*a*

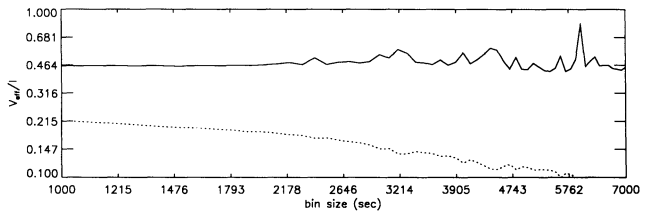

FIG. 2*b*

FIG. 2.—Fractional Effective Variability. The fractional effective variability for various bin sizes, ranging from 1 to 20 ks. The solid line is the effective variability as computed from the data, and the dotted line represents the effective variability that would be detected at a confidence level of 95%. We calculate the effective variability for two distinct intervals defined from the behavior of the α TrA light curve (cf. Fig. 1; see text). (*a*) Data gathered during the "post-flare" phase of the light curve. Note that an effective variability ~0.1 is detected at greater than 95% confidence at bin sizes greater than 7 ks during this "quiescent" phase. (*b*) Data gathered during the "first-flare" and "second-flare" phases. Note that an effective variability ~0.5 is detected at high confidence levels.

In order to understand the transient behavior discovered above, we carry out spectral fits to the data. We generally extract the count spectrum with PROS, and use XSPEC to fit spectral parameters. In all spectral fits, we model the data only with Raymond-Smith thermal plasma emission (available in the spectral fitting package XSPEC [v. 8]) from an optically thin gas. We first present (see Fig. 3) the spectrum of the counts, along with their best-fit two-temperature thermal spectra for both time intervals considered above, as well as for the entire observation. We are unable to fit the spectra with single temperature thermal spectra, and any other reasonable, more complicated spectral models (such as three-temperature fits or two-temperature fits with different extinctions) do not improve the fits significantly. The parameters of the two-temperature fits for each of the cases considered are reported in Table 2. There are three points worth noting here: First, these spectral fits conclusively demonstrate the existence of very high temperature ($T > 10^7$ K) plasma on α TrA; second, there is very little difference in the fit parameters of temperature and column density for the three cases; and finally, the best-fit column density to the spectrum is remarkably close to previous determinations from UV data (see § 3).

We now investigate in greater detail the possibility of variations in the spectrum with time: By dividing our observation (see Fig. 1) into "pre-flare," "first-flare," "second-flare," and "post-flare" segments (the last being further divided further into two approximately equal intervals), we compromise between the twin demands of good temporal resolution and the necessity of having sufficient counts for obtaining well-constrained spectral fits. With this choice of subintervals, the total counts in each subinterval are 248, 1336, 373, 876, and 896; and the exposure times are ~2845, 7062, 3811, 8435, and 10,161 s, respectively. The results of the spectral fit are shown in Figure 4. We find no evidence for any significant temporal variation in either the absorbing column densities or the plasma temperatures over the period of the observations, and the variations in X-ray flux can be ascribed to corresponding variations in the emission measures.

As pointed out above, we cannot demonstrate this result directly at shorter time intervals, due both to the paucity of counts in many GTI segments and to the short timescale variability introduced by the spacecraft wobble. Attempts to fit the count spectra collected over these shorter time intervals by "fixing" certain parameters such as column density or temperature at "best-fit" values still result in fits with large errors in the other parameters due to the specific spectral response of the *ROSAT* PSPC, preventing us from drawing firm conclusions about changes in the fit parameters. We can, however, show that this result is most likely valid at shorter time intervals by considering the evolution of the hardness ratio of the counts,

$$R(E; E_0, E_1) = \frac{C(E_1 - E)}{C(E - E_0)}, \quad (1)$$

where $C(E_i - E_j)$ are the counts in the passband $(E_i - E_j)$ keV in a given time interval. We take the time interval to be a GTI for simplicity. Examining the evolution of $R(E; 0.17, 2.02)$ for various values of E in the range 0.28–1.4 keV (see Fig. 5), we find that we consistently obtain reduced χ^2 values ~1 when fitting the ratios with models of constant hardness ratios. Thus, our results indicate that only changes in the emission measure are responsible for the flare events. This is significantly different from solar flares, for which the differential emission measure (DEM) at high temperatures ($T \gtrsim 1$ keV) shows a large increase relative to the "quiescent" DEM (see Figs. 2 and 3 of Bruner & McWhirter 1988). In contrast, the ratio of high- and low-temperature component emission measures lies in the range ~1–3 for α TrA. Spectral fits to the active stars have revealed ratios of similar magnitude for other active stars (cf. Schmitt et al. 1990), albeit with much greater scatter. These fits, however, do not distinguish between the "flaring" and "non-flaring" phases, and hence cannot be compared to our observations directly. We note, however, that single-temperature fits to stellar flares (e.g., Reale et al. 1988) show a large increase in the plasma temperature during the flare, suggesting behavior similar to that seen on the Sun. On the other hand, recent analysis of dM and dMe stars detected with *ROSAT* appear to contradict this point (Giampapa 1993).

Finally, we note that spectral fits to the five subintervals described above allow a determination of the count-to-energy conversion factor: each count corresponds to $(7.8 \pm 0.58) \times 10^{-12}$ ergs cm^{-2} at Earth, or equivalently, to $(5 \pm 0.6) \times 10^{29} (d/32 \text{ pc})^2$ ergs at the star.

2.2.2. ι *Aur*

ι Aur is a very weak X-ray source and was not detected during SASS processing. Therefore, we exclude durations of high background rates from data (i.e., those times when the spacecraft pointing was close to the terminator, resulting in high count rates due to O v fluorescence in the atmosphere), and explicitly excise sources detected during SASS processing from background estimation. We also limit our analysis to the energy range 0.28–2.02 keV, thus avoiding much of the instrumental background while still maximizing the range for com-

parison with α TrA.[6] Then, we compute net counts and the significance of the detection (determined as the probability that the observed number of net counts *cannot* be obtained as a Poisson fluctuation of the background counts) at various positions within the likely error circle around the predicted position of ι Aur. The mean position obtained from these calculations lies ≈11″ away from the predicted position. As discussed in § 2.1, these errors are comparable to the pointing accuracy of the spacecraft (Micela et al. 1994). Unfortunately, as with α TrA, there is no way to estimate the positioning errors independently within the field of view, as there is only one other X-ray source in the image that is unambiguously identifiable with an optical object, and that source is at a position nearly 40′ off-axis and has a centroid offset from the predicted position by 25″. Thus, our results indicate a detection of ι Aur in the X-ray region.

Owing to the small number of counts from ι Aur (∼21), we are unable to carry out a formal spectral fit. Hence, we use instead the ratio of counts in different passbands to constrain the properties of the X-ray–emitting plasma. The observed hardness ratio at a given energy E keV, $R(E; 0.28, 2.02)$ (see eq. [1]), is compared to a grid of ratios $R(T, N_H, E; E_0, E_1)$ obtained for thermal spectra of temperature T and extinction N_H as seen through the PSPC. For each N_H, we then obtain the range of T consistent with $R(E; 0.28, 2.02)$ and its error. The results are plotted in Figure 6 for a representative value, $E = 0.77$ keV (results for other values of E, for which the 1 σ errors in $R(E, 0.28, 2.02)$ are less that 100%, are similar to that shown in Fig. 6). We immediately see that the absorption column density is not constrained, but the plasma temperature is restricted to values in excess of a few million degrees for reasonable absorption column densities. This is consistent with the fact that ι Aur is detected in the high-energy bandpass.

[6] These two changes are the reason that the backgrounds estimated for the two stars are so different (cf. Table 2). The O v fluorescence contributes ≳30 counts and spillover of low-energy photons from the source circle contributes ≳50 counts to the estimated background of α TrA. In addition, ι Aur is located toward the Galactic anticenter, while α TrA is much closer to the direction of the Galactic center, implying different contributions from the diffuse background (cf. Kashyap et al. 1992b).

3. PREVIOUS OBSERVATIONS

We discuss previous observations of α TrA and ι Aur in this section. We discuss previous X-ray detections in § 3.1 and UV observations in § 3.2. We summarize the stellar parameters we have adopted in § 3.3 and briefly discuss the column density of absorption determined from UV observations in § 3.4.

3.1. *X-Ray Observations*

3.1.1. α *TrA*

Until the launch of the *ROSAT Observatory*, only α TrA was known to be an X-ray source: it was detected with *EXOSAT* in the 0.04–2 keV passband (Brown et al. 1991). The observed count rate of 3.3×10^{-3} counts s^{-1} corresponds to fluxes ranging from $(0.7–8.6) \times 10^{-13}$ ergs s^{-1} cm^{-2} (for assumed plasma temperatures ranging from $10^{5.5}$ to $10^{7.1}$ K) in the wavelength band 1.3–300 Å (∼0.04–10 keV). This compares well with the fluxes we derive here from *ROSAT* observations for the "quiescent" period. Brown et al. did not detect variabil-

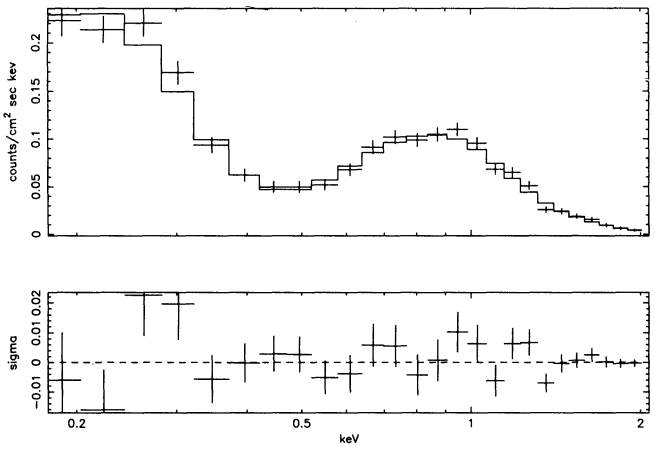

FIG. 3*a*

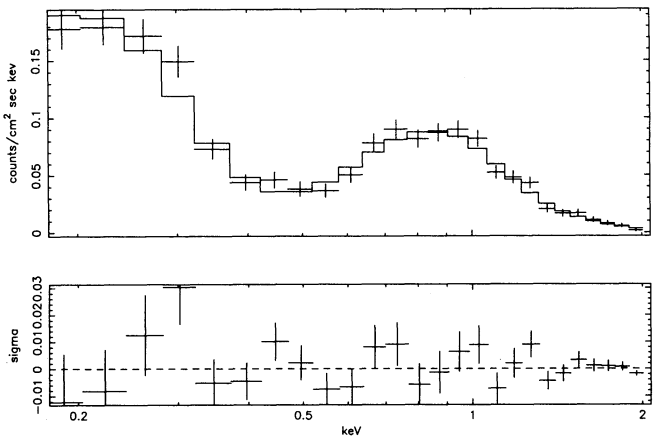

FIG. 3*b*

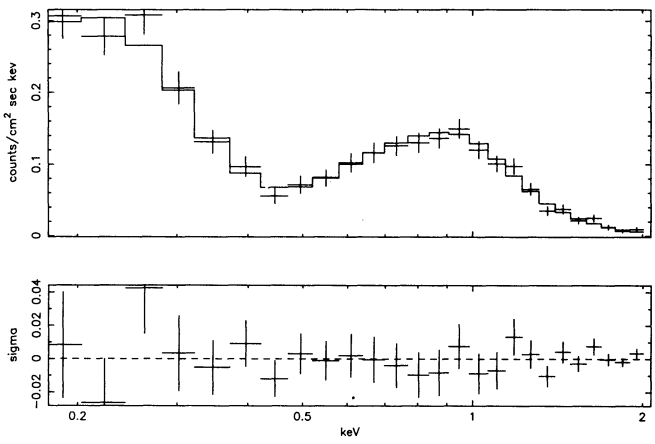

FIG. 3*c*

FIG. 3.—Count spectra of α TrA. The binned spectra of counts obtained through the PSPC are plotted in the upper panel. The plus signs mark the position of the observed count rates in each bin, with the vertical arms denoting the 1 σ errors associated with them. The solid line represents the best-fit two-temperature model spectrum (see Table 2). The lower panel depicts the departure of the observed counts from the best-fit spectrum in units of σ. (*a*) Data from the entire observation. (*b*) Data from the "quiescent" phase of the light curve (see Fig. 1). (*c*) Data obtained during the interval when the flares are identifiable in the light curve (see Fig. 1).

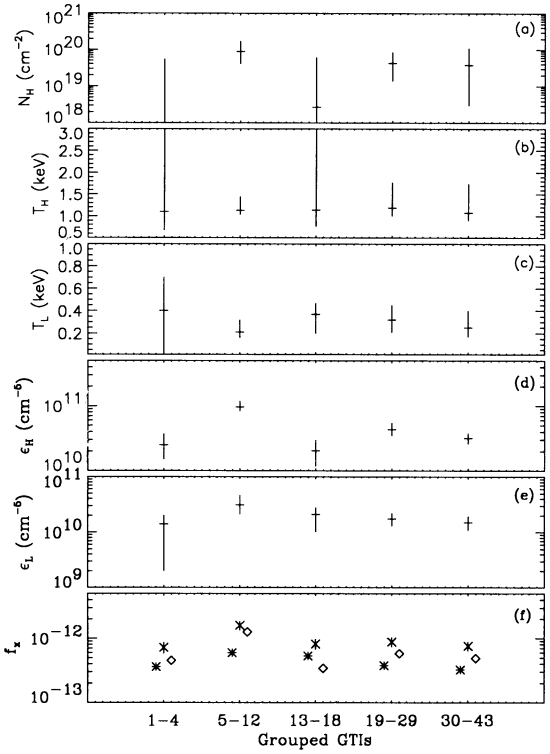

FIG. 4.—Evolution of fit parameters of α TrA. Temporal evolution of spectral fit parameters for the five temporal observing subintervals shown in Fig. 1 are displayed here. The parameters are (from top to bottom panels): (*a*) The absorbing column density (N_H, cm^{-2}); (*b*) The high-temperature component (T_H, keV); (*c*) The low-temperature component (T_L, keV); (*d*) The normalized emission measure for the T_H component, (ϵ_H, cm^{-5}); (*e*) The normalized emission measure for the T_L component, (ϵ_L, cm^{-5}); (*f*) The X-ray fluxes at Earth (f_X, ergs s^{-1} cm^{-2}). Crosses denote fluxes obtained by multiplying the count rate by the counts-to-energy conversion factor = $(7.8 \pm 0.58) \times 10^{-12}$ ergs cm^{-2} count^{-1}, Fluxes determined for the best-fit high (*diamonds*) and low (*asterisks*) temperature components are also shown, offset for clarity. We also show (via vertical bars) the upper and lower 90% confidence intervals for N_H, T_H, T_L, ϵ_H, and ϵ_L, and the 2 σ limits on the fluxes determined from the count rates. Note that the lower confidence limits on the column density and the upper confidence intervals for the temperature can at times be undefined because of the particular spectral response characteristics of the PSPC.

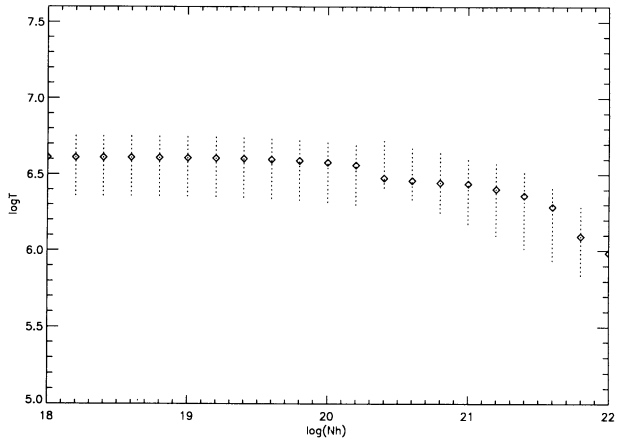

FIG. 6.—Spectral analysis of ι Aur. Plasma temperature and column densities consistent with the observed ι Aur hardness ratio R(0.77; 0.28, 2.02) are plotted. The diamonds represent the value of the temperature and column density of a single-temperature, optically thin plasma, which emits a thermal spectrum whose hardness ratio matches the observed ratio. The vertical dotted lines represent the uncertainty in the determination of the temperature at each value of the column density due to 1 σ errors in the determination of the observed ratio. Note that column density is *not* well constrained by this analysis, but for reasonable values of the column density (as determined from UV observations), the observed ratios signify the existence of multimillion degree plasma on ι Aur.

ity in their 23 ks (6.4 hr) observation, but this is not surprising, owing to the small number of counts.

During the *ROSAT* All-Sky Survey (Haisch, Schmitt, & Rosso 1992), α TrA was again detected, in both the soft (0.1–0.28 keV) and hard (0.5–2 keV) passbands of the PSPC. The observed count rate of 0.136 count s^{-1} corresponds to a flux of 8×10^{-13} ergs s^{-1} cm^{-2} for assumed plasma temperatures in excess of 10^7 keV and insignificant absorption. Again, this compares well with our flux determinations. The relatively high count rate seen in the survey has, however, a large statistical error of ≈36% associated with it and hence is still consistent with the count rates we observe.

3.1.2. ι *Aur*

In contrast to α TrA, ι Aur has not been previously detected in X-rays. Brown et al. (1991) placed an upper limit of

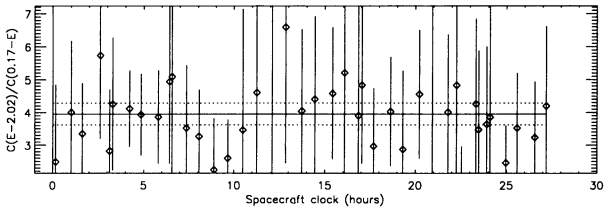

FIG. 5*a*

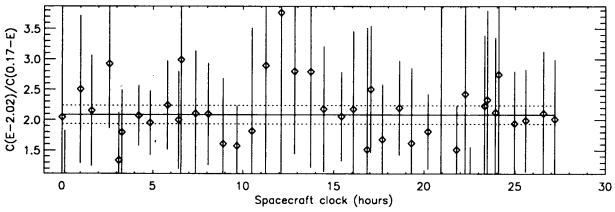

FIG. 5*b*

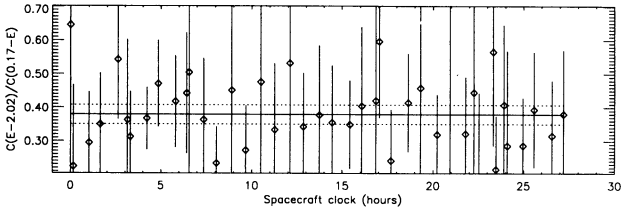

FIG. 5*c*

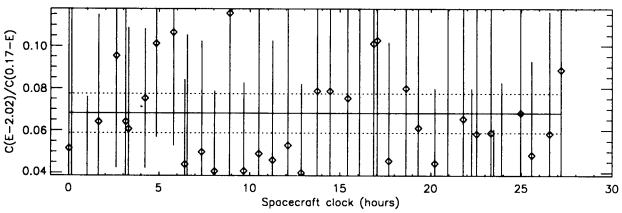

FIG. 5*d*

FIG. 5.—Evolution of hardness ratios for α TrA. Hardness ratios, calculated for each GTI, are plotted against the mid-segment time elapsed since the beginning of the observation (as in Fig. 1). The diamonds represent the values of the ratios, and the solid vertical lines represent the corresponding 2 σ errors. For comparison, we also plot the hardness ratio computed for the entire observation (*solid horizontal line*) along with its associated 2 σ errors (*dotted lines*). (*a*) The hardness ratio R(0.28; 0.17, 2.02); (*b*) The hardness ratio R(0.42; 0.17, 2.02); (*c*) The hardness ratio R(0.99; 0.17, 2.02); (*d*) The hardness ratio R(1.41; 0.17, 2.02).

1.7×10^{-3} counts s^{-1} during their 18 ks (5 hours) *EXOSAT* observation, corresponding to upper limits of (0.3–4.3) $\times 10^{-13}$ ergs s^{-1} cm^{-2}, scaled from their analysis of α TrA. This upper limit is obviously much higher than the actual flux we observed.

Haisch, Schmitt, & Rosso (1992) also attempted to detect ι Aur during the *ROSAT* All-Sky Survey, but failed, placing an upper limit of 2×10^{-13} ergs s^{-1} cm^{-2} in the 0.1–2.4 keV passband. A better limit of 4×10^{-15} ergs s^{-1} cm^{-2} was derived from a pointed observation lasting 10.64 ks (3 hr) conducted by Reimers & Schmitt (1992) using *ROSAT*. This is of the same order of magnitude as our detection (the slightly lower upper limit quoted by Reimers & Schmitt can be attributed to source count statistics or differences in the determination of the background or the spectral shape assumed in converting from counts to ergs).[7]

3.2. *UV Observations*

Both α TrA and ι Aur have been observed extensively in the UV region with the *IUE*. Both stars exhibit transition region and chromospheric emission lines (cf. Hartmann et al. 1981; Reimers 1982). We list some of these lines and the corresponding fluxes (see Table 3) for both α TrA and ι Aur. Note that the N V (1240 Å) line does not have a well-determined flux measurement, and the number quoted is actually an upper limit to possible detected emission (Hartmann et al. 1985). Using these fluxes, and the X-ray/UV-line flux correlations found by Haisch et al. (1990), we can predict the X-ray flux we should see from these stars. We find that X-ray fluxes ranging from 2–5×10^{-13} ergs s^{-1} cm^{-2} are expected for α TrA, while X-ray fluxes ranging from 1–5×10^{-14} ergs s^{-1} cm^{-2} are expected for ι Aur. The correlations found by Haisch et al. were between *IUE* line fluxes in C IV (1550 Å), Si IV (1400 Å), C II (1335 Å) and X-ray fluxes obtained with the *Einstein Observatory*. Comparing these predicted fluxes to observed X-ray fluxes, we find that α TrA is well behaved in terms of these correlations, while ι Aur is underluminous in X-rays by nearly an order of magnitude. Recently, Ayres (1993) found that the X-ray detected Hybrid stars (with the exception of α TrA) lie on a "depressed" X-ray/C IV (1550 Å) relation compared to the relation found by Haisch et al. (1990). This "depressed" relation apparently also matches the fluxes obtained for giant stars in the Hertzsprung gap, and if confirmed, would be of importance to theories explaining X-ray or chromospheric emission from Hybrid stars. Meanwhile, we note that it appears quite impossible to fit both α TrA and ι Aur on a single line relating X-ray and UV line fluxes. This implies a radical change in the mechanism of X-ray production between these stars (the UV line fluxes are within factors of 3–5 of each other for these stars, while the X-ray fluxes differ by more than two orders of magnitude), as suggested by Rosner et al. (1994; see § 4.4). Finally, we note that the He II (1640 Å) line is expected to be a good tracker of the X-ray emission (Hartmann, Dupree, & Raymond 1980; A. Dupree 1993, private communication), but it is hard to estimate the flux in this line without contamination from O I in low-dispersion *IUE* spectra (see below). Estimations of line fluxes from *HST* spectra would enable us to explore this issue further, particularly in the case of ι Aur.

[7] Reimers & Schmitt (1992) actually find a "slight excess of the observed photon count over the expected background" in the case of ι Aur, but since this excess was not statistically significant, they quote a 90% confidence upper limit.

TABLE 3

UV EMISSION-LINE FLUXES

Line	Wavelength (Å)	α TrA ($\times 10^{-13}$ ergs s^{-1} cm^{-2})	ι Aur ($\times 10^{-13}$ ergs s^{-1} cm^{-2})
C IV	1549	4.8	0.8
C II	1335	2.9	0.45
Si IV	1400	2.7	1.0
N V	1240	2.4	0.65
He II + O I	1640	2.6	0.8

Surface emission measures were derived from the UV line fluxes for both α TrA and ι Aur by Hartmann et al. (1985), who predicted upper limits $\sim 9 \times 10^{25}$ cm^{-5} for α TrA based on estimates of He II (1640 Å) emission in high-dispersion *IUE* spectra, and $\sim 3.6 \times 10^{25}$ cm^{-5} for ι Aur by scaling from α TrA. We obtain surface emission measures ranging from 4–15×10^{25} cm^{-5} during our observation of α TrA, which compares well with the value derived by Hartmann et al. The corresponding value for ι Aur is $\sim 5 \times 10^{23}$ cm^{-5}, which is well below the value predicted.

Finally, following Haisch et al. (1990), we calculate the surface filling fractions[8] of C IV for α TrA to be ~ 0.9 and for ι Aur to be ~ 0.5, assuming a density $\sim 10^9$ cm^{-3}. Such large values are consistent with the picture of the stellar surface being dominated by magnetic fields organized on a small spatial scale (see below).

3.3. *Stellar Parameters*

The precise spectral classification of α TrA has not been established. The measured parallax of 0".031 (cf. Kovács 1983) is consistent with the designation K4III, but the errors in the measurement are large enough to include the possibility that the star is twice as distant, consistent with the Ca II equivalent width and a designation of K4II. Here we nominally accept the parallax measurement placing α TrA at 32 pc, thus assigning the type K4III, and explicitly indicate this assumption in all calculations. Our understanding of the evolutionary history of the star is strongly dependent on the adopted spectral type, but the calculations carried out here are not. We list the stellar parameters we have adopted for α TrA in Table 4A (we show the values dependent on both distance estimates), and those for ι Aur in Table 4B.

3.4. *Absorption Column Density*

A good estimate of the interstellar absorption column densites toward α TrA and ι Aur does not exist, complicating our efforts to interpret the observed absorption. Both stars exhibit asymmetric Mg II line profiles indicating mass loss, and efforts to determine the column of material in the stellar wind of α TrA have resulted in values that differ by more than factors of 2. No major effort has been made to determine the absorption in the wind of ι Aur accurately as yet.

The first estimate of the absorption column in the stellar wind of α TrA was derived from the blueshifted absorption seen in the Lyα profile at -85 ± 20 km s^{-1} by Hartmann et al. (1981). They estimated the column density to be 2×10^{19}

[8] We use the corrected value of the power emitted, $P_{C\,IV}(T) \sim 1.5 \times 10^{-25}$ ergs cm^3 s^{-1}, which is smaller by a factor of 4π from the number obtained from Raymond & Doyle (1981). This correction is due to an error in the normalization of the intensity of the spectral line (Jordan 1992; see eq. [2] of Raymond & Doyle 1981).

TABLE 4

STELLAR PARAMETERS

A. α TrA

Parameter	Value	Comments
Spectral type	K4 III/II	[a]
Apparent magnitude, v	$1^m.92$	Haisch 1987
$B-V$	1.44	Haisch et al. 1990
Parallax, π [arcsec]	0.031	Kovács 1983; Haisch 1987
Angular diameter, ϕ [arcsec]	0.012	Harper 1992
Distance, d [pc]	32/73	[a]
Stellar radius, $R_*/R_\odot$	41/94	[a]
M_V	−0.6/−2.4	[a]
$T_{\rm eff}$ [K]	4100	[b]
$L_{\rm bol}$ [ergs s^{-1}]	$1.7/8.6 \times 10^{36}$	[a]
$M_{\rm bol}$	−1.8/−3.6	[a], based on $M_{\rm bol,\odot} = 4.76$
$l_{\rm bol}$ [ergs s^{-1} cm^{-2}]	1.35×10^{-5}	Apparent luminosity
$(R_*/d)^2$	8.5×10^{-16}	[c]
Surface gravity, g [cm s^{-2}]	28	[b]
Stellar mass, M_* [$M_\odot$]	1.8/9	[a]
Scale height at 10^5 K [cm]	5.94×10^{11}	[d]
Absorption column density [cm^{-2}]	5×10^{19}	...
Escape velocity, $v_{\rm esc}$ [km s^{-1}]	127/192	[a]

a We quote values dependent on both the lower distance estimate of 32 pc as well as the higher distance estimate of 73 pc.

[b] From model atmospheres fitting (Kovács 1983).

[c] Ratio of observed flux to stellar flux.

[d] Critical height for coronal "hot" loop solutions to exist (Antiochos et al. 1986).

B. ι Aur

Parameter	Value	Comments
Spectral type	K3 II	...
Apparent magnitude, v	$2^m.02$	Haisch 1987
$B-V$	1.53	Haisch et al. 1990
$V-R$	1.06	Haisch et al. 1990
$R-I$	0.82	Haisch et al. 1990
Angular diameter, ϕ [arcsec]	0.0074	Harper 1992
Distance, d [pc]	69	...
Stellar radius, R_* [$R_\odot$]	55	Harper 1992
M_V	−1.5	...
$T_{\rm eff}$ [K]	4046	Harper 1992
$L_{\rm bol}$ [ergs s^{-1}]	2.8×10^{36}	...
$M_{\rm bol}$	−2.4	based on $M_{\rm bol,\odot} = 4.76$
$l_{\rm bol}$ [ergs s^{-1} cm^{-2}]	4.9×10^{-6}	Apparent luminosity
$(R_*/d)^2$	3.2×10^{-16}	...
Surface gravity, g [cm s^{-2}]	50	Harper 1992
Stellar mass, M_* [$M_\odot$]	5.5	...
Scale height at 10^5 K [cm]	3.3×10^{11}	...
Absorption column density [cm^{-2}]	5×10^{19}	...
Escape velocity, $v_{\rm esc}$ [km s^{-1}]	195	...

cm^{-2}. The poor quality of the spectra precluded a more detailed analysis. Later, Hartmann et al. (1985) detected stellar winds at speeds up to −180 km s^{-1} in deep exposures of Mg II lines, but were unable to derive a column density for the material in the wind. Brown et al. (1991) then assumed that all the absorption seen in the Lyα profile was due to interstellar absorption, and obtained a best-fit column density of 5×10^{19} cm^{-2}. They divided the observed profiles by attenuations for different column densities, and decided on the goodness of fit by checking for the smoothness of the final result. This approach naturally cannot distinguish between the interstellar and wind components. Recently, Harper (1992) modeled the chromospheres and transition regions of α TrA and ι Aur, and noted that the wind column density required from Mg II column densities is of the same order (5×10^{19} cm^{-2}) as the interstellar hydrogen column density in both these stars. Tantalizingly, the best-fit absorption column densities derived from spectral fits to X-ray data from α TrA (see Table 2) range from 3–6 × 10^{19} cm^{-2}. It is therefore of considerable importance to determine the actual column density in the stellar winds, as distinct from interstellar absorption. To this end, T. R. Ayres (1993, private communication; Ayres & Kashyap 1994) recently reanalyzed *IUE* data for α TrA and estimated a total absorption of 3×10^{19} cm^{-2}, with two parts from the wind (at −80 km s^{-1}) and one part from the interstellar medium. Obtaining a good fit to the Lyα profile, however, requires the addition of an ad hoc component with a high velocity dispersion. The origin and implications of this component are as yet unknown.

4. DISCUSSION

4.1. *Does α TrA Have a Dwarf Companion?*

It has been suggested (Linsky 1993) that the flares seen during our observations of α TrA may actually arise on a hitherto unobserved low-mass dwarf companion to α TrA; this

suggestion is based on the similarity in the magnitudes of the flare X-ray luminosity ($L_X \sim 10^{29}$ ergs s^{-1}), emission measure (EM $\sim 10^{52}$ cm^{-3}) and temperature ($T > 10^7$ K) of the α TrA flares to those observed on late-type flare stars. This suggestion can never be rejected with certainty on the basis of the X-ray data alone, but a detailed comparison with the observed properties of flare stars show that it is very unlikely that these flares occur on a previously unobserved dK or dM star. Pallavicini, Tagliaferri, & Stella (1990) have conducted an extensive survey of X-ray flares observed on UV Ceti-type flare stars by *EXOSAT*, and identify two types of flare phenomena: *Impulsive* flares with rise times of a few minutes and decay times of tens of minutes, similar to compact loop flares on the Sun; and *long-decay* flares with decay times of 1 hr or longer, similar to two-ribbon flares on the Sun. Since the decay times (i.e., *e*-folding times) observed here are greater than 3 hours, the events we see cannot be "impulsive" flares; hence, we are left with the possibility that the α TrA flares are "long-decay" flares. First, we note that in none of the observations exemplifying the *long-decay* flare is the *e*-folding decay time much greater than 1 hr. Thus, the α TrA flares have exceptionally long decay times when compared to flares on low-mass main-sequence stars. This point is especially important because the dK/dM flares with longer decay times are typically "complex" (e.g., Haisch, Strong, & Rodonò 1991; see also the X-ray light curves shown in Pallavicini et al.), in the sense that they all show signs of multiple, successive events on timescales less than 1 hr. We, however, see no such complicating features in the light curve of α TrA, thus providing partial support for the argument that these flares are very distinct from dK/dM flares. Furthermore, modeling of dK/dM flares (e.g., Reale et al. 1988) shows a large increase in the temperature of the plasma during the flare event, suggesting that the differential emission measure (DEM) changes dramatically during the flare (see § 2.2.1). But in the case of the α TrA flares, while there is some evidence for changes in the DEM (as evidenced by changes in the relative emission measures of the high- and low-temperature components), these changes are only by factors $\sim$2–3 (see Fig. 4). Thus, it appears that while the α TrA flares resemble dK/dM flares superficially, they differ substantially in detail. Finally, estimates of the neutral H column density (including a $\approx$50% contribution from the stellar wind) toward α TrA obtained from *IUE* data (Brown et al. 1991; Harper 1992) closely coincide with the value derived here from spectral fits to the X-ray data ($N_{\rm H} \sim 5 \times 10^{19}$ cm^{-2}). This suggests a common origin for both, and there is little doubt (see below) that the UV emission is from α TrA. For all of these reasons, we believe that it is extremely unlikely that the observed transient emission arises from an unseen, low-mass main-sequence companion of α TrA.

We also note in passing that Ayres (1985) postulated that α TrA has a companion of spectral type dF based on an apparent excess of UV emission compared to α Boo. However, as pointed out by Brown et al. (1991) and Hartmann et al. (1985), α TrA has an energy distribution in the UV that is typical of Hybrid stars. Hence, following them, and in the absence of further evidence to the contrary, we will assume that all the UV emission seen arises from α TrA, and not from a dF companion.

4.2. *X-Ray Emission from α TrA*

In this section we discuss the physical implications of the spectral and temporal variability analysis we carried out for α TrA (cf. § 2.2).

4.2.1. *Coronal Plasma Number Density*

The observed exponential decay of the flares allows us to place limits on the electron number density (n_e) of the flaring, X-ray–emitting plasma. First, following Pallavicini, Tagliaferri, & Stella (1990), we equate the observed emission decay timescale of $\sim$3 hr (cf. § 2.2.1) with the timescale of radiative loss (thus ignoring loss due to conduction), $\tau_{\rm rad} = 3k_B\, T_e/n_e\, P_{\rm rad}(T_e)$, where $P_{\rm rad}(T_e)$ is the radiative loss for unit emission measure at temperature T_e, and thus derive an upper limit (see Table 2) $n_e \lesssim 10^{10}$ cm^{-3}. Alternately, we can set an upper limit on the number density from the *non*-detection of a decay in the plasma temperature (cf. § 2.2.1). Even though the *ROSAT* PSPC is not sensitive to changes in temperature around 10^7 K, we would be able to detect a drop from 1.5×10^7 K to (say) 5×10^6 K. Such a decrease is *not* observed, leading us to conclude that the temperature decay timescale (τ_T) is greater than the observed decay timescale. Following Veck et al. (1984), we use the energy equation in the case that the total number of particles in the loop vary,

$$3k_B n_e \frac{dT_e}{dt}\left(1 - \frac{2}{3}\frac{\tau_T}{\tau_n}\right) = -\frac{A}{V}\kappa T_e^{5/2}\frac{dT_e}{ds} - 0.8\ \mathrm{EM}\ P_{\rm rad}(T_e)\,, \tag{2}$$

where τ_n is the number density decay timescale, V is the emission volume, and A is the cross-sectional area of the loop; we also assume that the entire variation in X-ray flux is due to changes in the emission measure, and that the volume of emission remains constant; τ_n is then twice the observed decay timescale. Again ignoring the loss due to conduction, we obtain an upper limit $n_e \lesssim 10^{10}$ cm^{-3}, as before.

Deriving a lower limit on n_e is much more difficult. By requiring that $dT_e/dt < 0$ in equation (2), we can place an upper limit on the temperature decay timescale, $\tau_T < (3/2)\tau_n$, and hence place a (trivial) formal lower limit, $n_e > 0$. A more useful bound may be obtained by equating the decay timescale to the timescale of conductive loss (ignoring radiative loss) $\tau_{\rm cond} = (3k_B/\kappa)(n_e L_c^2/T_e^{5/2})$, where $\kappa = 9 \times 10^{-7}$ ergs s^{-1} K^{-1} cm^{-1} and L_C is a length scale characterizing the temperature gradient. Setting L_C to the possible height of the loop (clearly an overestimate, and likely to be unrealistically large due to the complex structure of the loop; cf. Pallavicini et al. 1990), $\sim 10^{11}$ cm [an estimate obtained by assuming that the plasma fills the loop over the observed flare rise times, $\tau_{\rm rise} \lesssim 1$ hr, $L \sim c_s(T_e)\tau_{\rm rise}$; note that the loop semilength derived below is consistent with this value], we obtain a lower bound of $n_e \gtrsim 10^9$ cm^{-3}. These values are comparable to the electron number densities derived for the transition region (Hartmann et al. 1985; also see Harper 1992). This result, together with the values of the emission measure obtained through spectral fits, allows us to estimate the volume of the flaring plasma.[9]

[9] We have assumed throughout that the flare dynamics is dominated by the higher temperature component, since the dominant emission component is that associated with the higher temperature component (denoted with subscript H; cf. Fig. 4), which would therefore dominate the observed cooling. On the other hand, the fluxes emitted by the two components are comparable in magnitude. Hence, our simplified picture is not capable of explaining the detailed evolution of the flares. However, for purposes of establishing the geometry of the emission, we assume the high-temperature component is the nominally dominant one. An effort to constrain the flare parameters by detailed model fitting (including heating, which is ignored here) is in progress (Reale et al. 1994).

4.2.2. *Geometry of Transient Emission*

The volume of the X-ray–emitting gas is $V_H = 4\pi d^2 \epsilon_H / n_e^2$ (where $\epsilon_H \equiv \mathrm{EM}_H / 4\pi d^2$, with EM_H the high-temperature emission measure and d the distance to the star). At the observed peak of the flare, $\epsilon_H = 1.5 \times 10^{11}$ cm^{-5}, so that the volume of the emitting plasma is given by

$$V_H = 1.2 \times 10^{32} \left(\frac{d}{32 \text{ pc}}\right)^2 \left(\frac{n_e}{10^{10} \text{ cm}^{-3}}\right)^{-2} \text{cm}^3 . \quad (3)$$

Assuming that the flare occurred within a single, semicircular, solar-like loop with an aspect ratio a ($\equiv$ loop radius/loop semilength), we obtain the semilength of the loop,

$$L \sim 1.4 \times 10^{11} \left(\frac{a}{0.1}\right)^{-2/3} \left(\frac{d}{32 \text{ pc}}\right)^{2/3} \left(\frac{n_e}{10^{10} \text{ cm}^{-3}}\right)^{-2/3} \text{cm} . \quad (4)$$

At the time of "quiescent" emission (for which the emission measure in the high-temperature component is $\epsilon_H \sim 3 \times 10^{10}$ cm^{-5}), the volume of the emitting plasma,

$$V_H \approx 3.7 \times 10^{31} \left(\frac{d}{32 \text{ pc}}\right)^2 \left(\frac{n_e}{10^{10} \text{ cm}^{-3}}\right)^{-2} \text{cm}^3 , \quad (5)$$

corresponds to a loop semilength,

$$L \approx 8 \times 10^{10} N^{-1/3} \left(\frac{a}{0.1}\right)^{-2/3} \left(\frac{d}{32 \text{ pc}}\right)^{2/3} \times \left(\frac{n_e}{10^{10} \text{ cm}^{-3}}\right)^{-2/3} \text{cm} , \quad (6)$$

where N is the number of discrete (identical) loops contributing to the X-ray emission (we assume $N \approx 1$ during the flare). For $N \lesssim 10$, such loops are large by solar standards, but are small when the large stellar radius ($R_* = 41.5\ R_\odot$) and the low surface gravity ($g = 28$ cm s^{-2}, corresponding to a scale height of 5.94×10^{11} cm at $T = 10^5$ K) are taken into account; for $N \gg 10$ (the more likely case), these loops are yet smaller. Thus, it is unavoidable (for reasonable choices of d, a, N, and n_e) that these loops violate the stability criterion of Antiochos, Haisch, & Stern (1986), viz., that the ratio, θ, of the gravitational scale height at 10^5 K to the height of the loop should be less than 1 in order that stable "hot" loop solutions exist. Indeed, $\theta \sim 4$ at the peak of the flare, and increases to $\sim 7N^{1/3}$ after the flare, so that θ is clearly substantially greater than unity during the "quiescent" phase.[10]

4.2.3. *Plasma Confinement*

It is well known that plasma at temperatures $\gtrsim 0.5$ keV cannot possibly be gravitationally confined on the surface of giants and supergiants (cf. Rosner, Golub, & Vaiana 1985). It is therefore gratifying to find that the magnetic field required to contain the plasma on α TrA is quite small: Setting $B^2 \gtrsim 8\pi p_g$, where the gas pressure, $p_g = 2n_e k_B T$, we find $B \gtrsim 30$ G for $n_e \sim 10^{10}$ cm^{-3} and $T \sim 15$ MK. In contrast, for UV Ceti-type flare stars, one obtains minimum confining magnetic fields over 500 G (Mullan 1989; Pallavicini, Tagliaferri, & Stella 1990). Thus, the confinement constraint imposes relatively weak demands on the magnetic fields on α TrA.

4.2.4. *Energetics*

The average X-ray luminosity observed in the interval during which the two flares occur is $\sim 9.6 \times 10^{28} (d/32 \text{ pc})^2$ ergs s^{-1}. Hence, the energy input to the corona (through the two loop footpoints) during the flare is

$$\gtrsim 1.5 \times 10^8 \left(\frac{d}{32 \text{ pc}}\right)^2 \left(\frac{a}{0.1}\right)^{-2} \left(\frac{L}{10^{11} \text{ cm}}\right)^{-2} \text{ergs s}^{-1} \text{ cm}^{-2} , \quad (7)$$

where the lower bound is established by assuming that the footpoints have the same cross-sectional area as the coronal loop itself. This is roughly three orders of magnitude larger than the mean energy input to the stellar wind (Holzer & MacGregor 1985), as calculated for a mass-loss rate of 10^{-9} $M_\odot$ yr^{-1}. Thus, these transients are well-described by the term "flare." Note that this result remains valid even for the duration when only small-amplitude transients are seen, consistent with our earlier finding that even the apparently "quiescent" X-ray emission is due to transient emission.

4.3. *X-Ray Emission on ι Aur*

The lack of sufficient counts to perform useful spectral fitting for ι Aur prevents us from drawing conclusions with the same robustness as with α TrA. However, if we make some reasonable assumptions regarding the origin of the X-ray emission, we can deduce the values of various quantities of interest.

The X-ray flux at Earth[11] from ι Aur is $\sim 6.1 \times 10^{-15}$ ergs s^{-1}. This corresponds to an observed X-ray luminosity of $\sim 1.8 \times 10^{27}$ ergs s^{-1}, comparable in magnitude to the upper limit derived from the *ROSAT* All-Sky Survey (Reimers & Schmitt 1992).

The power emitted per unit emission measure by a gas at $\sim 3 \times 10^6$ K, such as that found on ι Aur, is $\sim 4.5 \times 10^{-23}$ ergs cm^3 s^{-1} (from an analytical fit to the Raymond-Smith thermal emission; Chun & Rosner 1993). Hence, the volume emission measure of the hot material is $\sim 10^{50}$ cm^{-3}. Assuming an electron number density, $n_e = 10^9$ cm^{-3}, we find that the volume of the emitting plasma is $\sim 10^{32}$ cm^3, corresponding to a loop semilength

$$L \sim 1.2 \times 10^{11} N^{-1/3} \left(\frac{d}{69 \text{ pc}}\right)^{2/3} \left(\frac{n_e}{10^9 \text{ cm}^{-3}}\right)^{-2/3} \left(\frac{a}{0.1}\right)^{-2/3} \text{cm} , \quad (8)$$

where all the symbols have the same meaning as in § 4.2. No matter how many loops are involved (i.e., no matter what the value of N, $N > 1$), this is again less than the critical length defined by the scale height of the atmosphere at 10^5 K (for ι Aur, this critical length is 3.3×10^{11} cm), implying that the X-ray emission arises in one or more transient loops (see above). However, if we choose a value such as $n_e \sim 2 \times 10^6$ cm^{-3}, which is consistent with the gas pressure in the transition region ($n_e T \sim 10^{13}$ cm^{-3} K; see Harper 1992), we find that the loop semilength, $L \sim 7 \times 10^{12} N^{-1/3}$ cm, is much

[10] We have continued to use the nominal value of 10^{10} cm^{-3} for the electron number density in the X-ray–emitting loops during the "quiescent" phase, since we detect variability on timescales of order of hours (see § 2.2.1), and since the cooling continues to be dominated by plasma at the high-temperature component (see Fig. 4), thus ruling out low values of n_e. Note, however, that even for $d = 73$ pc, $n_e = 10^9$ cm^{-3}, we still have $L \sim 6 \times 10^{11} N^{-1/3}$ cm, and $\theta \gtrsim 1$.

[11] We adopt the same count-to-energy conversion factor for ι Aur as was determined from spectral analysis of α TrA, namely, 7.8×10^{-12} ergs cm^{-2} count^{-1}. This assumption is justified, since ι Aur does have high-temperature emission akin to α TrA (see § 2.2) and the column densities of absorption to the two stars are similar ($\sim 5 \times 10^{19}$ cm^{-2}).

greater than both the critical length and the radius of the star ($R_* = 54.8\ R_\odot$) unless the number of identical loops contributing to the X-ray emission is very large. We cannot rule out such a scenario based on *ROSAT* measurements, but with substantially more sensitive observations, one can constrain such models by using fluctuations during "quiescent" periods (as we have done in the case of α TrA).

As expected, the energy input at the base of the loop depends strongly on the geometry adopted for the X-ray emission. If we assume that the loops are small and unstable, we find that the energy input is $\sim 2 \times 10^6 N^{-1/3}$ ergs s^{-1} cm^{-2}, which is slightly greater than the energy required to maintain the stellar wind ($\sim 8 \times 10^5$ ergs s^{-1} cm^{-2} for a mass loss of $10^{-9}\ M_\odot$ yr^{-1}); and if we assume that the loops are highly extended, we find that only $\sim 300 N^{-1/3}$ ergs s^{-1} cm^{-2} are required.

Finally, we note that as with α TrA, we find that the magnetic field required to confine the plasma is small: $B > 8$ G in the case of high-pressure, compact loops, and $B > 0.3$ G in the case of low-pressure, extended loops (see above).

4.4. *Comparison with Models*

Five mechanisms have been proposed to explain the drop in X-ray emission across the Dividing Line as well as to explain the coincidence of the Wind and Coronal Dividing Lines: (1) low transition region densities, leading to low emission measures for X-ray emission in coronae (Linsky & Haisch 1979); (2) extinction of coronal emission by a high-density wind (cf. Maggio et al. 1990); (3) a change in the character of the coronal loops such that only cool loops (with $T < 10^5$ K) are stable (Antiochos, Haisch, & Stern 1986); (4) a change in the structure of the magnetic fields to an open topology, leading to a decrease in the amount of high-temperature plasma that is magnetically confined (Linsky & Haisch 1979; see also Rosner et al. 1991); and (5) a change in the character of the magnetic dynamo, leading to the disappearance of fields organized on the stellar length scale found on the Dividing Line, leaving only small-scale, turbulence-generated fields to the right of the Line (Rosner et al. 1994), and thus causing a natural transition in the topology of the magnetic fields.[12] We consider each in turn.

Low Density Corona: The idea that a low density in the transition region would lead naturally to much lower densities at coronal distances, and hence low emission measures for X-ray emission, was proposed by Linsky & Haisch (1979) as an alternative to the possibility that stars without observable X-ray emission have no coronae. However, as pointed out by Rosner et al. (1991), giant stars cannot have a multimillion degree hot gas without magnetic confinement, for otherwise, the gas would expand freely at velocities much higher than those observed. Hence, this model must be considered a refinement of the one involving the topology of the magnetic fields, and cannot by itself provide a complete picture of the phenomenon. Also, given the low X-ray flux from ι Aur, this model would predict a comparatively low flux in transition region lines compared to α TrA, which is contradicted by *IUE* observations (Hartmann et al. 1985; see § 3.2).

Absorption of Coronal Emissions: The intensity of X-ray emission at the source is not considered in this model, where the large column densities provided by massive outflows are thought to be the main reason for the drop in X-ray emission across the Dividing Line. However, as pointed out by Maggio et al. (1990), there is no evidence of increased absorption on red giants as compared to typical F and G giants. Recently, Haisch, Schmitt, & Fabian (1992) computed the amount of absorption expected from cool winds on stars to the right of the Dividing Line, and found that the attenuation caused by the wind is not enough to account for the observed drop in X-ray emission. Finally, this model is unable to explain the difference in the X-ray emissions from α TrA and ι Aur: if ι Aur were assumed to have an X-ray luminosity 40% that of α TrA (Hartmann et al. 1985; based on emission measure analyses of *IUE* observations—see above), the absorption column density required to cause the "observed" attenuation would be $\gtrsim 10^{22}$ cm^{-2} (cf. Table 2 of Haisch, Schmitt, & Fabian 1992). This is more than two orders of magnitude greater than the estimated column density to ι Aur. We therefore support Haisch, Schmitt, & Fabian (1992) and Maggio et al. (1990) in their conclusion that this model cannot account for the existence of the Dividing Line.

Cool Loops: A drop in X-ray emission can also be effected if the temperature of the corona is forced to a low value ($\sim 10^5$ K). This situation may occur in stars where the loop sizes are smaller than the density scale height at 10^5 K (Antiochos, Haisch, & Stern 1986; see also Antiochos et al. 1985; Antiochos & Noci 1986). In such cases, the only stable loop solutions possible are those of "cool" loops with a maximum temperature $\sim 10^5$ K. Since the density scale height increases with decreasing gravity, there will be regions of the H-R diagram where the loop sizes drop below the critical loop length for which cool solutions are preferred, causing a steep decline in the X-ray emissions. This region was identified with the location of the Dividing Line by Antiochos et al. (1986). For α TrA, the density scale height at 10^5 K is $\sim 6 \times 10^{11}$ cm, and for ι Aur, it is $\sim 3 \times 10^{11}$ cm, and steady X-ray emission requires loop sizes to be greater than these values for the respective stars. However, even at the peak of the flare on α TrA, the height of the loop is only ~ 1–2×10^{11} cm, and during the "quiescent" period, it drops to $\sim 8 \times 10^{10} N^{-1/3}$ cm (see § 4.2.1). Values for ι Aur are also consistent with this assertion. Thus, it appears that all the emission on Hybrid stars must be due to flaring loops. Indeed, in conjunction with the model of changing magnetic topology proposed by Rosner et al. (1994; see also Rosner et al. 1991), this paradigm can account for most of the observed properties of our program stars (see below).

Change in Magnetic Field Topology: As suggested originally by Linsky & Haisch (1979; subsequently extended by Rosner et al. 1991), a change in the magnetic field structure across the Dividing Line, from a closed to an open topology as in a solar coronal hole, would lead to a decrease in the amount of hot gas confined to the star, and hence, to a decrease in X-ray emission. In other words, the surface filling fractions of active regions decrease across the Dividing Line. (A mechanism for accomplishing this is not provided for in this model.) As a by-product of

[12] We distinguish between the fourth and fifth models for two reasons. First, the former model does not impose a specific mechanism for the change in the topology of magnetic fields, and hence must be considered independent of any proposed mechanism. In other words, the validity of the basic paradigm, viz., the change in the topology of the field, must be evaluated independently of models to *explain* this change. We note that this requirement reduces the testability of the model and also note that naive application of the model produces a contradiction with observations. Hence a model that incorporates a mechanism for changing the topology is *required* (see below). Second, the model proposed by Rosner et al. (1994) incorporates several features that produce testable effects other than the change in topology, and hence must be considered separately.

this decrease, the effectiveness of Alfvén wave reflection increases (Rosner et al. 1991), leading to increased wind flow across the Dividing Line. Thus, magnetic confinement of hot plasma and cool stellar winds are naturally anticorrelated. Rosner et al. used the ratio α of the stellar radius to the density scale height as a measure of the efficacy of Alfvén wave reflection in an open field topology. Giants with cool winds uniformly have $\alpha > 20$, while giants with chromospheric emission uniformly have $\alpha < 10$. For both α TrA and ι Aur, $\alpha \gg 20$ for reasonable parameters of distance and temperature. Recently, Lou & Rosner (1994) obtained three-dimensional solutions for Alfvén wave propagation in isothermal, hydrostatic, spherically symmetric stellar atmospheres and calculated the reflection coefficients at various frequencies for different values of α. Their idealized analysis is valid close to the stellar surface, where temperatures ~ 1–5×10^4 K are the norm (see the chromospheric model calculated by Harper 1992). For the parameters of interest, this is the temperature range at which significant wave trapping starts to occur for both α TrA and ι Aur. For example, all frequencies below 10^{10} Hz are trapped (i.e., the transmission coefficient drops to ~ 0.1) at 2×10^4 K in ι Aur. This trapping has two important consequences: First, it deposits momentum at the base of the wind, thus increasing the mass flux; and second, it reduces the amplitude of the Alfvén waves propagating into the wind, thereby decreasing the Alfvén wave energy density and consequently the effect of Alfvén waves on the structure of the wind at large distances.[13] Hence, mass loss increases from left to right across the Dividing Line, while X-ray emission decreases. Thus, this model provides a unified explanation for the practical coincidence of the coronal, chromospheric and wind dividing lines (cf. Ayres et al. 1981). However, a mechanism that accomplishes the change in the topology of the magnetic field is not specified in this model, and consequently, it cannot be compared with observations in detail. For instance, using this model, naive expectations of the magnitude of X-ray emission as scaled from the observed UV emissions for α TrA and ι Aur are not confirmed by our observations. Indeed, the surface filling fractions of C IV are similar in magnitude for both stars (see § 3.2), leading us to expect similar values for the sizes of the active regions, and hence for the X-ray emission. Instead, X-ray observations lead us to think of α TrA as being dominated by closed field regions to a significantly greater extent than ι Aur. Further, there is no reason a priori to expect that the loop heights should be less than the critical height required for stability (see above). We will consider an enhancement of this model which explains these points in the next paragraph.

Change in the Magnetic Dynamo: Most recently, Rosner et al. (1994) proposed a paradigm to explain the change in the topology of the magnetic fields. They contend that as a star crosses the Dividing Line in the course of its evolution, a transition occurs in the character of the magnetic dynamo causing the activity: $\alpha - \omega$ type dynamos, which are responsible for the generation of large-scale fields that can confine plasma at high temperatures (and thus provide X-ray emission at detectable levels), cease to exhibit growth; instead, the magnetic fields on the stellar surface are generated by turbulent motions in the convection zones of these stars, thus generating small-scale fields which cannot confine large volumes of high-temperature plasma (resulting in a drop in the intensity of the X-ray emission).[14] The existence of the small-scale magnetic field to the right of the Dividing Line accounts for the observational coincidence of the lack of X-ray emission and the maintenance of steady stellar winds: Alfvén waves reflection due to the steep gradient in Alfvén speed (see above), leads to rapid acceleration of the stellar wind; further, the loops remaining on the surface of the star would be small, and unstable if they contained hot plasma. Thus, in the view of Rosner et al. (1994), giant stars undergoing the transition from being dominated by large-scale dynamo-driven activity (and solar-like X-ray emission properties) to being dominated by small-scale dynamo activity (and non-solar like X-ray emission properties) are identified with Hybrid stars. If we assume that α TrA and ι Aur are at the "early" and "late" stages of this transition, we can qualitatively account for the puzzling features of our observations, namely, the change in the correlation between the X-ray and C IV fluxes for the two stars and the temporal variability of the X-ray emission on α TrA. Due to the changing character of the magnetic fields during this transition, we should not expect the correlation between X-ray and C IV fluxes determined for giants on the left of the Dividing Line to hold for Hybrid stars, and indeed it does not. Furthermore, the dominance of magnetic fields closed on small scales ($\theta \gg 1$, see above) in Hybrid stars implies that steady "hot" coronal loops cannot exist, and any X-ray emission must arise in unstable loops, as is the case for α TrA. This instability naturally leads to the observed variability in the X-ray emission. Note that the model does not specifically predict the existence of flares, but does not rule out such high-energy events either.

5. SUMMARY

We report here on our observations of two Hybrid stars, α TrA and ι Aur, with the *ROSAT Observatory*. Our analysis of the data has resulted in a number of interesting conclusions:

We detect X-ray emission from both α TrA and ι Aur, the latter for the first time; these detections imply that Hybrid stars are X-ray emitters in general;

The detection of ι Aur in the high-energy passband of *ROSAT*, coupled with the observed values of the hardness ratios, imply the existence of multimillion degree plasma on ι Aur;

Spectral fits to the α TrA data unambiguously confirm the existence of high-temperature plasma ($T > 10^7$ K);

We detect X-ray flares for the first time from Hybrid stars (namely, on α TrA), and demonstrate that the flares arise from loops that are smaller than the density scale height of the atmosphere at 10^5 K;

The plasma characteristics during the clear flare events and during the "quiescent" phase on α TrA are indistinguishable,

[13] This is contrary to the suggestion of Hartmann & MacGegor (1980). Indeed, comparing the wind energy flux (~ 6–16×10^4 ergs s^{-1} cm^{-2} for α TrA, and $\sim 8 \times 10^4$ ergs s^{-1} cm^{-2} for ι Aur for a mass-loss rate of $10^{-9}\ M_\odot$ yr^{-1}; see Holzer & MacGregor 1985) to the Alfvén wave energy flux at the base of the flow (see Hartmann & MacGregor 1980), we find that the amplitude of the fluctuations in the magnetic field is $\sim 10^{-4}$ for a magnetic field of ~ 20 G, and a number density of $\sim 10^9$ cm^{-3}.

[14] Transition is thought to be a result of the despinning of the star at the Dividing Line, which in turn occurs due to magnetic braking via mass loss through a magnetized stellar wind. The sharp drop in activity is preceded by an increase in activity up to the Dividing Line, which causes enhanced X-ray emission and increased mass loss. There appears to be evidence for this enhanced activity in *Einstein* data (A. Maggio 1993, private communication), but it is not conclusive. A program to verify this using the *ROSAT* All-Sky Survey data is underway (Haisch et al. 1993).

suggesting that the underlying physical phenomena are fundamentally the same, but differ only in scale (e.g., amplitude);

The emission during the apparently "quiescent" phase of α TrA is also marked by considerable variability, suggesting that there is no quiescent X-ray coronal loop component in the atmosphere of α TrA;

The loop scale heights for the "quiescent" emission on α TrA are much shorter than the critical length (Antiochos, Haisch, & Stern 1986) required in order to obtain steady "hot" loop solutions.

A simple explanation of these results is that all the X-ray emission from hybrid stars derives from highly transient loop events—that is, that there is no truly quiescent coronal loop component in their atmospheres. Our study of the geometry of the X-ray–emitting plasma on α TrA shows that the likely dimensions of the confined hot gas both during the prominent flares and during the "quiescent" phase are smaller than required for the existence of stable hot coronal loops, as expected on the basis of the recent suggestion of Rosner et al. (1994) that hybrid stars constitute a physically meaningful "transition" across the X-ray dividing line in the H-R diagram, between giants with large-scale magnetic dynamo-driven activity (and solar-like X-ray emission properties) and giants dominated by small-scale dynamo activity (i.e., stars for which $\alpha - \omega$ type dynamos do not exhibit growth), and "open" atmospheres dominated by cool, slow winds and no X-ray emission of any sort. That is, hybrid stars can be viewed as objects that have begun the transition to dominance of relatively small-scale ($\theta \gg 1$) closed surface magnetic field structures, where—by the argument of Antiochos et al.—steady "hot" coronal loops cannot exist, but where the dynamical interaction between these small-scale magnetic loops remain sufficiently vigorous to drive coronal transients (flares).

Thus, our observations have provided the initial observational support to theoretical models used to explain the existence of the Dividing Line in the H-R diagram first identified by Linsky & Haisch (1979), and the existence of Hybrid-chromosphere stars first detected by Hartmann, Dupree, & Raymond (1980). Our analysis also suggests a course for future action:

1. Other Hybrid stars need to be observed at X-ray wavelengths with sufficient sensitivity that one can carry out time-resolved X-ray spectroscopy and thus further explore the comparison between large transients and the relatively "quiescent" background emission. This type of observation is necessary to confirm the results presented here.
2. Simultaneous UV and X-ray observations can in principle definitively eliminate the possibility that the observed transient emission (associated with α TrA here) comes from an as yet unseen low-mass companion star.
3. Other elements of the theoretical models must be tested, such as the prediction of increasing X-ray emission as a star evolves toward the Dividing Line, and the prediction of the existence of stellar winds even to the left of the Dividing Line.
4. The winds on Hybrid stars must be modeled to account for the curious observational features seen in *IUE* spectra.
5. Accurate distances, and hence spectral types, to Hybrid stars must be obtained, in order to remove the ambiguity that exists currently. Indeed, knowledge of the evolutionary history of a given star would greatly aid in deciding the emphasis laid on particular properties exhibited by these stars.
6. Hydrodynamic modeling of the flares on α TrA may help constrain the parameters defining the environment in which the flares occur and may be of help in resolving the identity of the X-ray source.

We thank Jeff Linsky, Jürgen Schmitt, Carole Jordan, Tom Ayres, and Andrea Dupree for their very useful comments, and Peter Freeman and Tom Metcalfe for assistance with variability analysis. This paper has been submitted in partial fulfilment of degree requirements at UC (V. K.). We would like to acknowledge support by the NASA *ROSAT* Guest investigator Program at the University of Chicago (V. K., R. R.), NASA contract NAS 5-30934 at SAO (F. R. H.), and Agenzia Spaziale Italiana, Ministero dalla Università e della Ricerca Scientifica e Tecnologica, and GNA-CNR in Italy (A. M., G. M., S. S.).

APPENDIX A

TEMPORAL VARIABILITY ANALYSIS

We carry out a temporal variability analysis of our data by comparing statistics derived from observed photon arrival times with those derived from assuming models with specific types of variability. We perform this exercise using the technique of Collura et al. (1987).

We first calculate the phase-averaged χ^2 statistic for the count rates at various binning intervals, b, by averaging the reduced χ^2

$$\chi^2_\nu(b, \phi) = \frac{1}{\nu} \sum_{i=1}^{n} f_i \frac{(c_i/f_i - I)^2}{I} \tag{A1}$$

over all phases ϕ, where f_i is the fraction of ON time during the ith of n intervals, $\nu = n - 1$ is the number of degrees of freedom, I is the expected counts in each bin, and c_i are the observed counts in each bin. The phase-averaged reduced x^2 statistic, $\chi^2_\nu(b)$, is only asymptotically χ^2 distributed. By considering the counts in each bin, c_i, as being due to the sum of a steady Poisson-distributed component $f_i \alpha_i$, and a variable component $f_i V_i$, an effective variability,

$$V^2_{\rm eff} = \langle V_i^2 \rangle - \langle V_i \rangle^2 - \langle V_i \rangle \tag{A2}$$

is obtained. $V_{\rm eff}$ is a measure of the departure of the variable part of the light curve from a Poisson-distributed "constant" count rate source. Thus, a fractional effective variability can be obtained as the measure of the variable component in the light curve

(Collura et al. 1987):

$$\frac{V_{\rm eff}^2}{I^2} = \frac{v}{n\langle f_i\rangle}\frac{[\chi_v^2(b) - 1 - g]}{I}, \tag{A3}$$

where $g = n\langle f_i\rangle/p - 1$ is a correction factor for gaps in the data. Note that I is calculated by averaging the observed counts over the bins and hence does not imply the existence of a component of constant intensity in the light curve. The quantity $V_{\rm eff}/I$ measures the departure of the variable component from a source with a fixed count rate and a Poisson count distribution.

The phase-averaged reduced χ^2 statistic used in this method is asymptotically χ^2 distributed. Hence, estimates of the confidence intervals on $V_{\rm eff}/I$ are formally correct only at large values of $\bar{\chi}_v^2(b)$, corresponding to detections of variability at confidence levels $\gtrsim 95\%$.

We can identify the existence of a dominant timescale if the fractional effective variability is decreased significantly beyond a particular value of the bin width, $b_{\rm crit}$. The timescale of variability is then $\sim b_{\rm crit}$.

REFERENCES

Antiochos, S. K., Haisch, B. M., & Stern, R. A. 1986, ApJ, 307, L55
Antiochos, S. K., & Noci, G. 1986, ApJ, 301, 440
Antiochos, S. K., Shoub, E. C., An, C.-H., & Emslie, A. G. 1985, ApJ, 298, 876
Ayres, T. R. 1985, ApJ, 291, L5
Ayres, T. R. 1993, private communication
Ayres, T. R., & Kashyap, V. 1994, in Proc. 8th Cool Star Workshop, in press
Ayres, T. R., Fleming, T. A., & Schmitt, J. H. M. M. 1991, ApJ, 376, L45
Ayres, T. R., Linsky, J. L., Vaiana, G. S., Golub, L., & Rosner, R. 1981, ApJ, 250, 293
Brown, A., Drake, S. A., Van Steenberg, M. E., & Linsky, J. L. 1991, ApJ, 373, 614
Bruner, M. E., & McWhirter, R. W. P. 1988, ApJ, 326, 1002
Chun, E., & Rosner, R. 1993, ApJ, 408, 678
Collura, A., Maggio, A., Sciortino, S., Serio, S., Vaiana, G. S., & Rosner, R. 1987, ApJ, 315, 340
Dupree, A. 1993, private communication
Giampapa, M. 1993, BAAS, 25(2), 827
Gregory, P. C., & Loredo, T. J. 1992, ApJ, 398, 146
Haisch, B. M. 1987, in Lecture Notes in Physics 291, Proc. 5th Cambridge Workshop on Cool Stars, Stellar Systems, and the Sun, ed. J. L. Linsky & R. E. Stencel (Berlin: Springer), 269
Haisch, B. M., Bookbinder, J., Maggio, A., Vaiana, G. S., & Bennett, J. O. 1990, ApJ, 361, 570
Haisch, B. M., Schmitt, J. H. M. M., & Fabian, A. C.1992, Nature, 360, 239
Haisch, B. M., Schmitt, J. H. M. M., Maggio, A., Kashyap, V., & Rosner, R. 1993, in preparation
Haisch, B. M., Schmitt, J. H. M. M., & Rosso, C. 1991, ApJ, 383, L15
———. 1992, ApJ, 388, L61
Haisch, B. M., Strong, K. T., & Rodonò, M. 1991, ARA&A, 29, 279
Harper, G. M. 1992, MNRAS, 256, 37
Hartmann, L., Dupree, A. K., & Raymond, J. C. 1980, ApJ, 236, L143
———. 1981, ApJ, 246, 193
Hartmann, L., Jordan, C., Brown, A., & Dupree, A. K. 1985, ApJ, 296, 576
Hartmann, L., & MacGregor, K. B. 1980, ApJ, 242, 260
Holzer, T. E., & MacGregor, K. B. 1985, in Mass Loss from Red Giants, ed. M. Morris & B. Zuckerman (Dordrecht: Reidel), 229
Jordan, C. 1992, private communication
Kashyap, V., Rosner, R., Harnden, F. R. Jr., & Maggio, A. 1992a, BAAS, 24, 1205
Kashyap, V., Rosner, R., Micela, G., Sciortino, S., Vaiana, G. S., & Harnden, F. R., Jr. 1992b, ApJ, 391, 667
Kovács, N. 1983, A&A, 120, 21
Linsky, J. L. 1993, private communication
Linsky, J. L., & Haisch, B. M. 1979, ApJ, 229, L27
Lou, Y.-Q., & Rosner, R. 1994, ApJ, 424, 429
Maggio, A. 1993, private communication
Maggio, A., Vaiana, G. S., Haisch, B. M., Stern, R. A., Bookbinder, J., Harnden, F. R., Jr., & Rosner, R. 1990, ApJ, 348, 253
Micela, G., Sciortino, S., Harnden, F. R. Jr., Kashyap, V., & Rosner, R. 1994, ApJ, submitted
Mullan, D. J. 1989, Sol. Phys., 121, 239
Pallavicini, R., Tagliaferri, G., & Stella, L. 1990, A&A, 228, 403
Poletto, G. 1989, Sol. Phys., 121, 313
Press, W. H., Flannery, B. P., Teukolsky, S. A., & Vetterling, W. T. 1986, Numerical Recipes (Cambridge: Cambridge Univ. Press)
Raymond, J. C., & Doyle, J. G. 1981, ApJ, 245, 1141
Reale, F., Peres, G., Serio, S., Rosner, R., & Schmitt, J. H. M. M. 1988, ApJ, 328, 256
Reale, F., Peres, G., Maggio, A., Kashyap, V., & Rosner, R. 1994, in preparation
Reimers, D. 1982, A&A, 107, 292
Reimers, D., & Schmitt, J. H. M. M. 1992, ApJ, 392, L55
Rosner, R., Golub, L., & Vaiana, G. S. 1985, ARA&A, 23, 413
Rosner, R., An, C.-H., Musielak, Z. E., Moore, R. L., & Suess, S. T. 1991, ApJ, 372, L91
Rosner, R., Musielak, Z. E., Cattaneo, F., Moore, R. L., & Suess, S. T. 1994, ApJ, submitted
Schmitt, J. H. M. M., Collura, A., Sciortino, S., Vaiana, G. S., Harnden, F. R., Jr., & Rosner, R. 1990, ApJ, 365, 704
Stencel, R. E., Mullan, D. J., Linsky, J. L., Basri, G. S., & Worden, S. P. 1980, ApJS, 44, 383
Trümper, J., et al. 1991, Nature, 579
Veck, N. J., Strong, K. T., Jordan, C., Simnett, G. M., Cargill, P. J., & Priest, E. R. 1984, MNRAS, 210, 443